Simulation of solar magneto-convection

R. Cameron, A. Vögler, and M. Schüssler

Max-Planck-Institut für Sonnensystemforschung[1]
Max-Planck-Str. 2, 37191 Katlenburg-Lindau, Germany
cameron,voegler,schuessler@linmpi.mpg.de

1 Introduction

The term 'magneto-convection' summarizes the variety of processes arising from the dynamic interaction between convective motions and magnetic fields in an electrically conducting medium. Magneto-convective processes play an important role in many astrophysical systems; their effects can be best studied in the case of the Sun, where the relevant spatial and temporal scales of the phenomena can (in principle, at least) be observed. The generation of magnetic flux in the Sun by a self-excited dynamo process and the various spectacular phenomena of solar activity, like sunspots, coronal loops, flares, and mass ejections all are, directly or indirectly, driven by magneto-convective interactions.

Realistic numerical simulations of solar magneto-convection represent a considerable computational challenge. The large length scales of the typical convective flow structures on the Sun lead to high (hydrodynamic and magnetic) Reynolds numbers, so that the magneto-convective processes typically involve nonlinear interactions and formation of structures and patterns. There is an extended range of length scales between the dominant scale of the convective flow pattern and the dissipation scales. The plasma is strongly stratified and even a restricted simulation has to cover a density ratio of the order of 100. Convective velocities reach the sound speed, so that full compressibility is mandatory. Solar convection is strongly affected by partial ionization effects, so that the ionization state of the most abundant species (foremost hydrogen) has to be monitored in the course of the simulation and the related contributions have to be incorporated into the equation of state.

The energetics of the lower solar atmosphere is strongly affected by radiative energy transport. The radiative transfer equation for the specific intensity of radiation has to be intergrated along a large number of rays of various angles in order to determine the radiation incident on each grid cell. In order

[1] formerly: Max-Planck-Institut für Aeronomie

to correctly represent the temperature field in the solar atmosphere, the frequency dependence of the radiation has to be taken into account. This further complicates the problem because about a million spectral lines contribute to the energy balance in the solar photosphere.

This report is organized as follows. We briefly describe the numerical methods and the code that we use to treat the equations of radiative magnetohydrodynamics in Sec. 2. Results of simulations are presented in Sec. 3: magnetoconvection with different amount of magnetic flux in Sec. 3.1 and simulations of a solar pore in Sec. 3.2. Our experience with the HLRB Hitachi SR8000-F1 is described in the concluding Sec. 4.

2 Numerical methods

We use the magnetohydrodynamic (MHD) approximation for a collision-dominated, electrically well-conducting, quasi-neutral plasma. These conditions are fairly well fulfilled in the convection zone and lower atmosphere of the Sun. The physical system is then described by the combination of the MHD induction equation, which governs the evolution of the magnetic field, with the equations of hydrodynamics including appropriate magnetic terms in the momentum equation (the Lorentz force) and in the energy equation (the Joule dissipation term). In addition, the energy equation contains a source term, which accounts for heating and cooling of the plasma by radiation.

For our simulations, we use the MURaM[2] code, which is a joint development of our group at the Max-Planck-Institut für Sonnensystemforschung (MPS) and the computational MHD group at the Dept. of Astronomy and Astrophysics of the University of Chicago [1, 2, 3, 4]. The MURaM code solves the combined equations of MHD and radiative transfer on a three-dimensional regular cartesian grid with constant grid spacing. The spatial derivatives are discretized with 4th-order centered differences on a 5^3 point stencil. Time stepping is explicit with a 4th-order Runge-Kutta solver. The scheme is stabilized by the application of shock-resolving diffusion and hyperdiffusivity [5], which prevent the build-up of energy at scales comparable to the size of the grid cells. These artificial diffusivities assume significant values only near discontinuities and in regions of unresolved waves while those regions which are well resolved remain largely unaffected by diffusion. For the equation of state the instantaneous ionization equilibrium for the first ionization of the 11 most abundant elements is considered. The relevant thermodynamic quantities are stored in tables, from which the required values are interpolated during a simulation run.

We describe the frequency dependence of the radiative transfer using the multigroup method [6, 7, 1]. The basic idea is to sort frequencies into 4 to 6 sets according to the geometrical depth in a 1D reference atmosphere at which

[2] **M**PS and **U**niversity of Chicago **Ra**diation **M**HD code

optical depth unity at that wavelength is reached. For each of these frequency sets, a radiative transfer equation with a set-integrated source function and a set-averaged opacity is solved. For averaging we consider the Rosseland mean (taken over the frequency set) in optically thick regions and make a smooth transition to the Planck mean in optically thin layers. The angular discretization is carried out using a quadrature formula with three directions per octant.

We solve the radiative transfer equation for each frequency set and each direction using the short characteristics scheme [8] with linear interpolation of opacity, source function and density along the rays together with bilinear interpolation of incoming intensity on cell boundaries. In the context of the domain decomposition used for parallelization, the short characteristics scheme requires an iteration for each ray direction and each frequency set. For a given ray direction the scheme starts in each subdomain at those boundaries through which the radiation enters (the 'upwind' boundaries). The intensity values at these boundaries are assumed to be known. Then the traversal of the subdomain proceeds in the downwind direction, systematically moving away from the upwind boundaries, thus making sure that the upwind intensities can always be determined by interpolation. However, on those upwind boundaries of a subdomain which do not coincide with the top or bottom boundary of the computational box, the intensities are a priori unknown. Therefore, the scheme is iterated until convergence at the boundaries is obtained. After each iteration the intensities at a given upwind boundary are updated with the new values provided by the neighbouring subdomain. We found that 2 to 3 iteration steps per frequency set and direction are usually sufficient, if one chooses as initial guess for the intensities on the upwind boundaries a linear extrapolation of the values of the previous two time steps.

The bottom boundary conditions implemented in the MURaM code permit free in- and outflow of matter and maintain a constant mass in the computational box as well as a fixed energy flux through the system. In the present version of the code, the top of the domain is closed with stress-free boundary conditions for the horizontal velocity components; the implementation of a more realistic transmitting upper boundary is under development. The magnetic field is assumed to be vertical at the bottom and either potential or vertical at the top boundary. The horizontal directions are taken to be periodic in all variables.

The code is parallelized by means of domain decomposition. The computational domain is divided into a three-dimensional array of subdomains, each of which is endowed with two layers of ghost cells at its boundaries as required by the 4th-order spatial discretization scheme. We use message passing (MPI) for parallel computers with distributed memory.

3 Simulation results

During the first 8 months of our HLRB project, we have started two studies with our 3D radiation MHD code MURaM running on the Hitachi SR8000-F1:

1. Dependence of solar magneto-convection on the amount of magnetic flux through the computational domain: a series of simulations with average vertical magnetic field between 10 G and 800 G.
2. Structure and dynamics of a small sunspot (solar 'pore'): what are the thermal and dynamical properties of a highly concentrated magnetic structure with a field strength of 2 kG and how does it affect the surrounding solar plasma?

3.1 Magnetic structure for different amount of flux

The solar atmosphere permits us to study magneto-convection in a variety of physical regimes, which are mainly characterized by the average magnetic field, B_0, corresponding to the amount of magnetic flux per unit area in the region considered. These regimes range from the weakly magnetized 'quiet Sun' with $B_0 \simeq 10\,\mathrm{G}$ to the dark core of a sunspot (the umbra) with values of B_0 up to 3000 G. Here we present results from an ongoing parameter study of solar magneto-convection with simulation runs for $B_0 = 10$, 50, 200 and 800 G, respectively. In all cases, the computational box corresponds to a small section of the solar photosphere and uppermost convection zone with a height of 1400 km (spanning the range between about 800 km below and 600 km above the visible solar 'surface', i.e., the surface of optical depth unity in the visible light) and a horizontal extension of $6000 \times 6000\,\mathrm{km}^2$, discretized with a spatial grid of $100 \times 288 \times 288$ points.

The simulations are started as non-magnetic convection. After the convection has fully developed and reached a statistically stationary state (about one hour solar time after the start of the simulation), a homogeneous vertical initial magnetic field of field strength B_0 is introduced and the further evolution followed for up to two hours, providing sufficient time to establish a statistically stationary magneto-convection pattern. For the 4 simulation runs considered here, Fig. 1 shows snapshots of various quantities in the fully developed state: vertical magnetic field (left) and vertical velocity (middle) on a horizontal plane corresponding roughly to the visible solar surface, together with the frequency-integrated brightness (right). The 'quiet Sun' run ($B_0 = 10\,\mathrm{G}$, top row) shows nearly undisturbed solar convection ('granulation') with the typical pattern of bright, isolated upflows and a network of dark convective downflow lanes. Within a time of a few minutes (corresponding to the turnover time of the convection pattern), several flux concentrations are assembled by the horizontal convective motions and appear in the downflow regions in the form of small bright points caused by the chanelling of radiation in the partially evacuated flux concentrations [3].

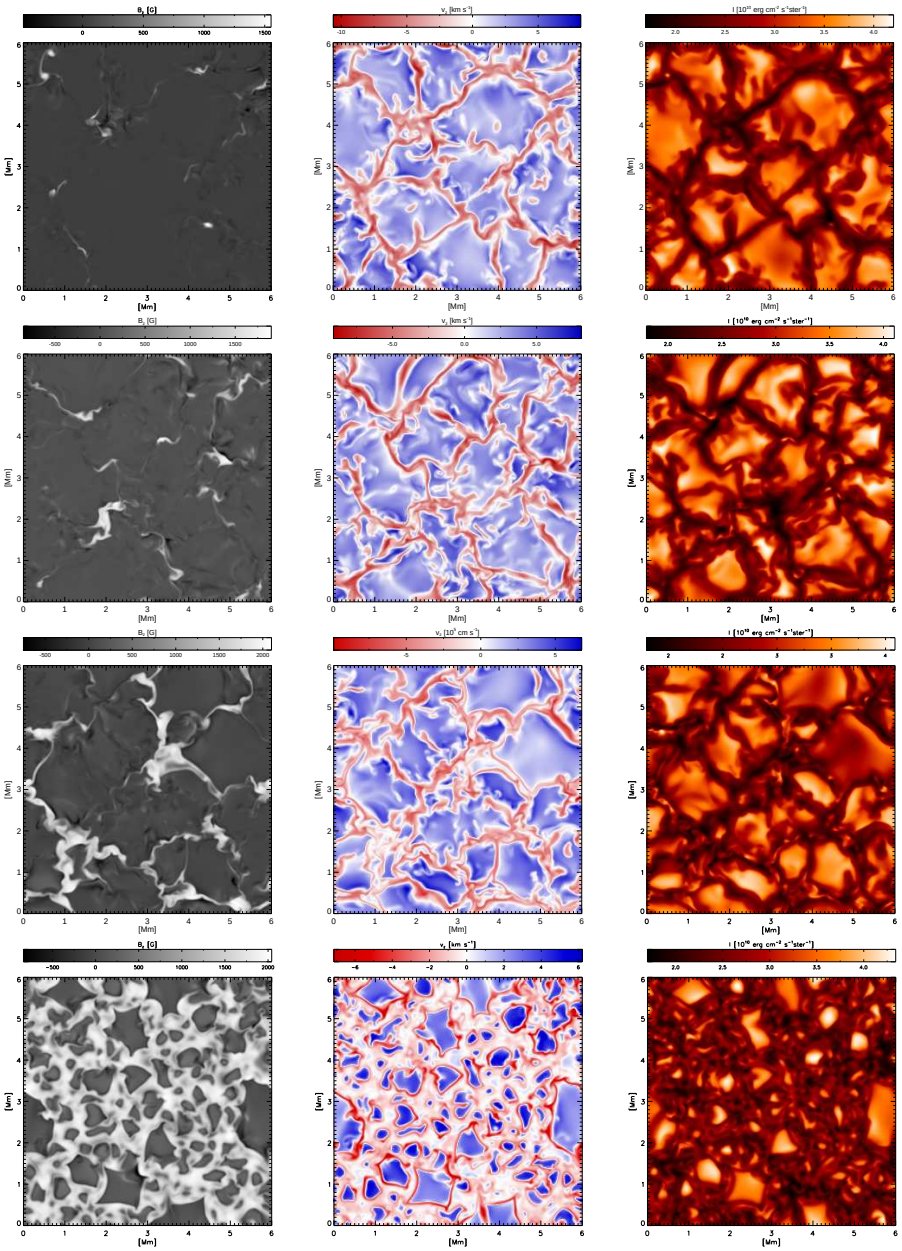

Fig. 1. Snapshots from simulation runs with $B_0 = 10\,\mathrm{G}$ (top row), $B_0 = 50\,\mathrm{G}$ (second row), $B_0 = 200\,\mathrm{G}$ (third row), and $B_0 = 800\,\mathrm{G}$ (bottom row). Shown are horizontal cuts near the visible solar surface of the vertical magnetic field component (left column), vertical velocity component (middle column), and brightness (frequency-integrated radiation intensity, right column).

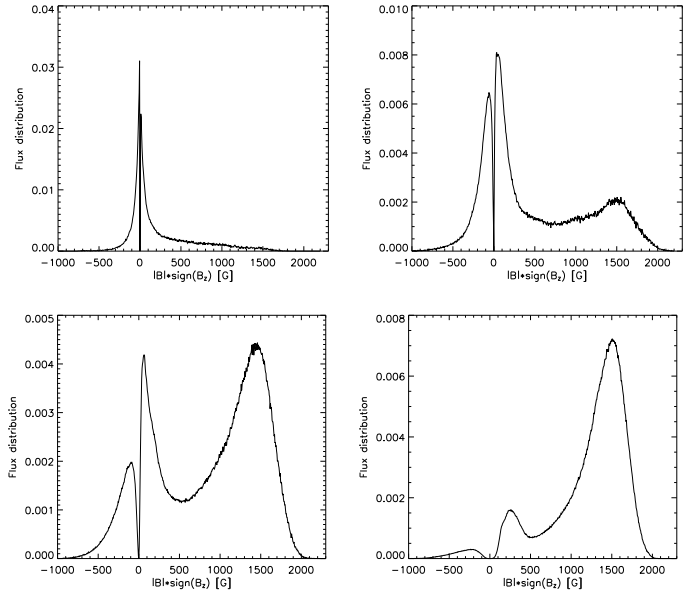

Fig. 2. Distribution over field strength of the unsigned vertical magnetic flux at the visible solar surface for simulation runs with various average vertical magnetic field strengths: $B_0 = 10\,\mathrm{G}$ (upper left), $B_0 = 50\,\mathrm{G}$ (upper right), $B_0 = 200\,\mathrm{G}$ (lower left), and $B_0 = 800\,\mathrm{G}$ (lower right). With increasing magnetic flux through the computational domain, a growing fraction of the flux is assembled in strong concentrations with kilogauss field strength.

For larger values of the magnetic flux through the region, many sheet-like magnetic structures form along the convective downflow lanes and larger structures with diameters of up to 1000 km appear at the vertices where several downflow lanes merge. Typical field strengths in these field concentrations are between 1500 G and 2000 G. The case $B_0 = 50\,\mathrm{G}$ (second row of Fig. 1) corresponds to a region in the solar magnetic network, where bright points are more numerous, while the case $B_0 = 200\,\mathrm{G}$ (third row of Fig. 1) represents a small part of a magnetically 'active region' on the Sun, which typically also contain sunspots and produce the various energetic phenomena of solar activity. This run also shows larger flux concentrations, which are darker than average because the radiation channeling in such structures cannot compensate for the suppression of the convective energy transport by the strong magnetic field. There is considerable small-scale variation of the intensity within these larger flux concentrations, which is related to localized hot upflows.

The disturbance of the convective flow pattern by the magnetic field, which is already visible in the case $B_0 = 200\,\mathrm{G}$, becomes rather severe in the case $B_0 = 800\,\mathrm{G}$ (bottom row of Fig. 1). The typical size of the hot upflows (granules) becomes much smaller because they have to 'squeeze' through the ex-

tended regions of strong magnetic field, which largely suppress the convective motions, while the strong downflows are restricted to narrow lanes surrounding the upflows. This situation is reminiscent to the case of a sunspot umbra, where isolated bright upflows ('umbral dots') appear in a dark background of almost stagnant, strongly magnetized plasma.

Fig. 2 shows the distributions of the unsigned vertical magnetic flux as a function of field strength for the various cases. While in the case $B_0 = 10\,\mathrm{G}$ most of the flux is in the form of weak field, a growing fraction of the flux is assembled in strong-field structures as B_0 increases. Eventually, in the case $B_0 = 800\,\mathrm{G}$ nearly all flux is in kilogauss form.

3.2 Structure and dynamics of a solar pore

Pores are magnetic features of a intermediate size. With a typical diameter of a few thousand km they are much larger than the small-scale flux concentrations in the magnetic network or in active regions and typically smaller then sunspots. They differ from sunspots in the absence of a penumbra, a region of long, narrow, dark and bright stripes directed outwards from the sunspot on the solar surface. They differ from the small-scale flux concentrations in that they appear dark at visible wavelengths.

Pores and sunspots form by the emergence of magnetic flux tubes from the deep parts of the solar convection zone, a process which cannot be easily incorporated in a numerical study of the layers near the surface. We therefore start our simulations with a pore already in place (a plug of kilogauss magnetic field) and investigate its structure and evolution until its eventual decay. We use a computational box of $12,000\,\mathrm{km}$ size in each of the horizontal directions and a height of $1400\,\mathrm{km}$ with a grid of 288×288 points in the horizontal directions and 100 grid points in height.

All the (vertical) sidewalls are treated as periodic. This is appropriate as long as the simulated pore occupies only a small fraction of the computational domain and thus feels little influence from the periodicity. Similar to the simulations described in the previous section, we use an open boundary condition at the bottom and a closed boundary condition at the top. Since the pore is a magnetically largely isolated structure, the choice of an upper boundary condition for the magnetic field is not obvious. We consider two limiting cases: a) purely vertical field and b) potential field. The former limit might be more appropriate early after formation, while the latter condition might be more realistic for the later stages, after the magnetic configuration has had time to relax. Below we compare the results for these two limiting cases. The main issue at the lower boundary is that strong magnetic fields inhibit convection and thus heat flow (this is why pores are dark). This effect also occurs outside the computational box, so that we reduce the internal energy density of inflowing material in magnetic regions (field strength above $180\,\mathrm{G}$).

Figure 3 shows a snapshot from a calculation with the vertical field boundary condition, taken approximately 1 hour after the simulation was started.

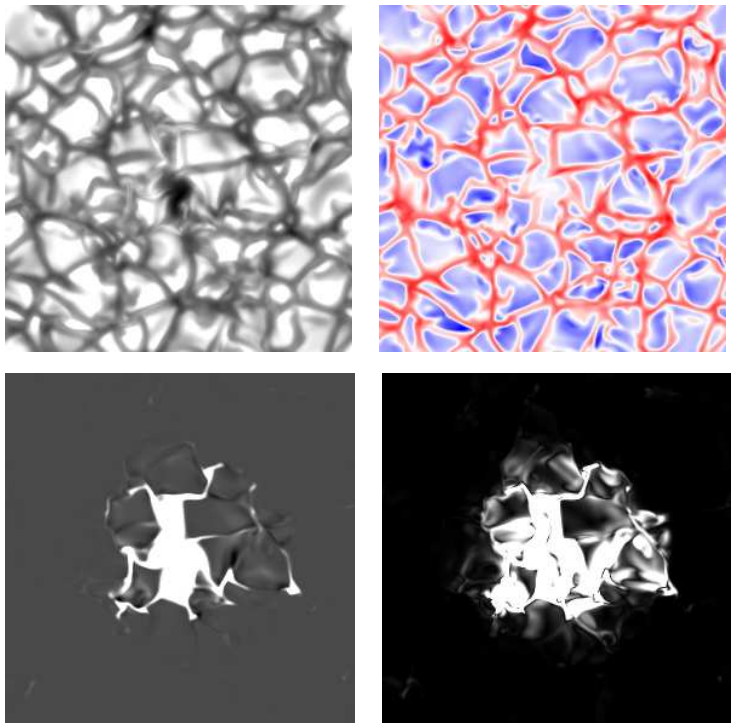

Fig. 3. Snapshot from a simulation of a solar pore with the vertical magnetic field boundary condition: brightness (upper left), vertical velocity (upper right), vertical component of the magnetic field (saturates at 1000 G, lower left), and magnitude of the horizontal magnetic field (saturates at 100 G, lower right), all quantities corresponding to the visible solar surface. The magnetic field images show only the central part containing the pore.

The pore is surrounded by a downflow, which prevents the magnetic structure from fragmenting. In contrast, the imposition of a potential field boundary condition leads to the rapid breakup of the pore. The strong vertical magnetic field covers not only the dark area in the intensity image, but also the bright walls corresponding to the downflow around the pore.

Our second boundary condition is to match the field at the top of the computational domain with a potential field. We start this simulation with a snapshot (after 45 minutes) from the simulation with the vertical field boundary condition. The potential field boundary condition means that the magnetic field spreads out very quickly with height, and thus we can expect more interaction between the magnetic field and the upper layers of the convective cells. Figure 4 is from a snapshot taken 10 minutes after the potential field boundary condition was imposed. The velocity streamline (shown in yellow) reveals helical motions with an axis perpendicular to the edge of the pore. This motion is driven by a large temperature gradient in the first few hundred kilo-

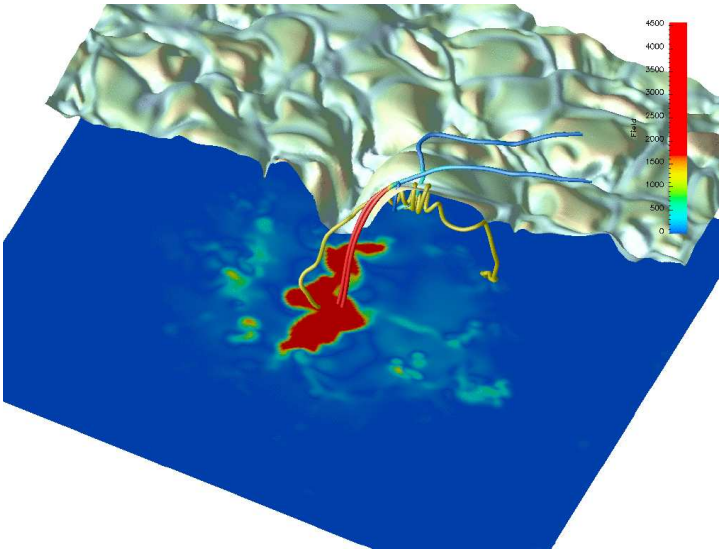

Fig. 4. Result 10 min after imposing the potential field boundary. The visible solar surface (optical depth unity) is coloured according to the emergent intensity. The vertical component of the magnetic field is displayed at the bottom of the box and along two field lines. A velocity streamline is shown in yellow.

meters beneath the visible surface. The magnetic field lines are transported and distorted by the flow: some arrive at a substantial angle to the vertical whilst others are pulled below the surface and emerge essentially vertically (but displaced from the pore). The field strengths are near or above equipartition with the kinetic energy density of the flow, implying that the magnetic field affects the motions. This type of structure, a type of convective roll, might be a precursor to a penumbral filament of a sunspot, which has similar features.

4 The MURaM code on the Hitachi SR8000-F1

The MURaM code is written in a mixture of ANSI C and C++. The code was originally developed for MPI-2, but we also have a version ported to MPI-1. At the time the code was first compiled on the SR8000-F1, there was only limited ANSI support for the then available Hitachi sCC compiler and Standard Template Library. We therefore compiled the MPI-1 version of the MURaM code using both the KAI and the GNU (g++ Gcc) compilers, in 64 bit mode (-m 64 -lmpi64). The code worked in both cases and the GNU compilers were chosen for efficiency for the production runs.

To determine the scaling with number of processors, some test cases were ran with 8, 32, and 256 processors. The total domain size was held constant

during these tests. The time taken per step (excluding start-up times and file operations) for the vertical magnetic field boundary condition scaled very close to inversely with the number of processors (to within a few percent), indicating that there were no communication bottlenecks. The scaling of the code implementing the potential field boundary condition was somewhat worse. We found a performance loss of about 10% when using 256 processors from what could have been expected from 8 processes and a linear scaling. A non-perfect scaling was expected because the potential field condition is a global condition, which we implemented with Fast Fourier Transforms. That the loss in performance is only 10% is in large part due to the fact that the rest of the code does most of the computational work, with the potential field only being evaluated at one boundary.

For the production runs, the jobs were typically sent to the parallel N32 queue to run on 256 processors. We found excellent turnaround times; in most instances our jobs began within 24 hours after submission. With 256 processors, each timestep takes approximately 12 seconds. As is to be expected, this equates to a per processor speed which is significantly lower than, for instance, those of IBM regatta processors. However, the large number of processors available and the fast turnaround times more than makes up for this. The time spent in I/O operations by our code is negligible in comparison with the computational time, so this aspect of its performance was not investigated.

References

1. Vögler, A.: Three-dimensional simulations of magneto-convection in the solar photosphere. PhD thesis, University of Göttingen (2003)
2. Vögler, A., Shelyag, S., Schüssler, M., Cattaneo, F., Emonet, Th., Linde, T.: Simulation of solar magneto-convection. In: N. E. Piskunov, W. W. Weiss, and D. F. Gray (eds) Modelling of Stellar Atmospheres, ASP Conf. Series, Astronomical Society of the Pacific, San Francisco, in press
3. Vögler, A., Schüssler, M.: Studying magneto-convection by numerical simulation. Astron. Nachr./AN, **324**, 399–404 (2003)
4. Schüssler, M.: Mhd simulations: what's next? In: J. Trujillo Bueno and J. & Sánchez Almeida (eds) Third International Workshop on Solar Polarization, ASP Conf. Ser., Astronomical Society of the Pacific, San Francisco, in press
5. Caunt, S. E., Korpi, M. J.: A 3D MHD model of astrophysical flows: Algorithms, tests and parallelisation. Astron. Astrophys, **369**, 706–728 (2001)
6. Nordlund, A.: Numerical simulations of the solar granulation. I - Basic equations and methods. Astron. Astrophys, **107**, 1–10 (1982)
7. Ludwig, H.-G., Jordan, S., Steffen, M.: Numerical simulations of convection at the surface of a ZZ Ceti white dwarf. Astron. Astrophys, **284**, 105–117 (1994)
8. Kunasz, P. B., Auer, L.: Short characteristic integration of radiative transfer problems: formal solution in two-dimensional slabs. J. Quant. Spectrosc. Radiat. Transfer, **39**, 67–79 (1988)